19

Analysis of Welding Residual Stresses and Its Applications

Byeong-Choon Goo, Jung-Won Seo and Seung-Yong Yang
Korea Railroad Research Institute
Korea

1. Introduction

Welding has been one of the most effective joining methods for structural steel from its advent in the middle of 1930s. Welding has increased productivity of shipbuilding, bridge building, construction, etc. Though welding has many advantages, it has several drawbacks such as welding deformation, residual stresses and welding defects. Regarding structural integrity, welding residual stresses are a key factor to be considered. A lot of study on welding residual stresses has been conducted in experimental and numerical areas, but the effect of the residual stresses on mechanical behavior, fatigue life, etc. has not been clearly explained until yet. Some results show the effect of welding residual stresses on fatigu e lives is significant. On the other hand, other results show specimens with tensile re sidual stress have even longer fatigue lives than parent materials. These unclear conclu sions seem to be mainly concerned with residual stress relaxation during fatigue tests and the metallurgical difference of the welded materials and parent materials. Therefore, understanding of residual stress relaxation by an applied loading is very important for fatigue life prediction and structural integrity analysis of welded structures. The improvement of numerical analysis methods has contributed very much to the understanding of role of residual stresses in weldments. In particular, finite element method (FEM) has been a powerful tool for analysis of welding process and related problems. In the following, we will deal with several numerical analysis problems concerned with welding. They are welding residual stresses, welding residual stress relaxation, residual stress effect on the fatigue and fracture of welding details. All finite element analyses were carried out by using ABAQUS code.

2. Analysis of residual stress relaxation due to mechanical loading

A lot of study on welding residual stress has been conducted in experimental (Iida and Takanashi, 1998) and numerical areas (Yang and Goo, 2005), but the effect of the res idual stresses on fatigue life has not been clearly explained until yet. In this study, we studied the residual stress relaxation by the finite element analysis. Initial residual stresses of a welded specimen were generated by the simulation of welding process. Residual stress relaxation under applied loading was examined by elastoplastic finite element analysis.

2.1 Generation of residual stress by welding

Two dimensional welding analyses are carried out to generate initial residual stresses in the plate shown in figure 1. Longitudinal welding is carried out along the middle line of the plate. The width of the weld bead is 4 mm. After welding, metallurgical structure is changed. In the experimental study (Iida and Takanashi, 1998), a large hole enough to rule out the effect of the metallurgical structure change is pierced. The process of hole drilling is simulated by using the element removal command. Figure 2 shows the finite element mesh. A half of the specimen is considered. The bottom of the specimen (y=-95) is fixed and longitudinal loading is applied to the opposite side. All finite element analyses were carried out by ABAQUS Code. Figures 3 and 4 show physical and material properties used for the simulation. A kinematic hardening rule was used. First of all, temperature field by welding is obtained. By using the temperature field, elastoplastic finite element analysis is performed. Finally the hole drilling analysis is carried out. The distribution of residual stress σ_{yy} along the x-axis from the hole center is shown in figure 5. Before the hole drilling, the maximum residual stress σ_{yy} is nearly the same as the yield stress of the base material. An interesting point is that after the hole drilling the residual stress increases.

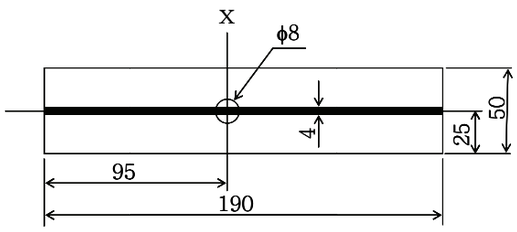

Fig. 1. Welded plate, thickness=4

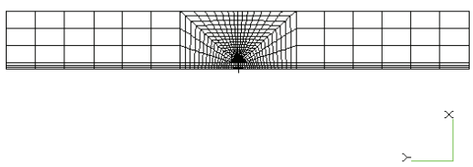

Fig. 2. Finite element model

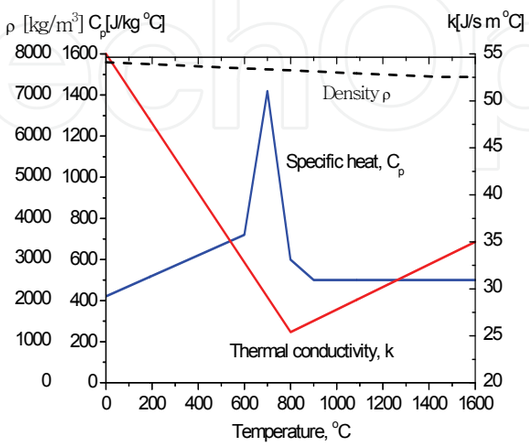

Fig. 3. Material properties: conductivity k, density ρ, and specific heat, c_p.

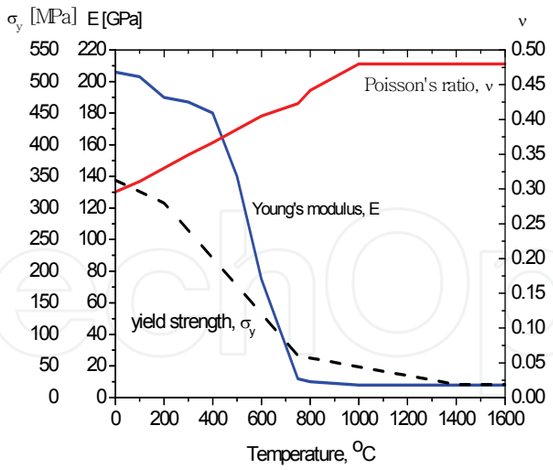

Fig. 4. Young's modulus E, Poisson's ratio ν, and yield stress σ_y

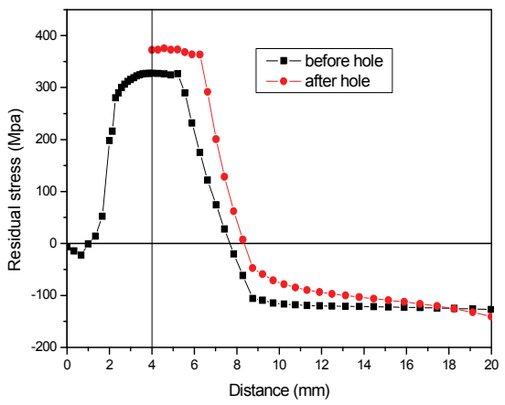

Fig. 5. Residual stress σ_{yy} before and after the hole drilling

2.2 Residual Stress Relaxation by applied loading

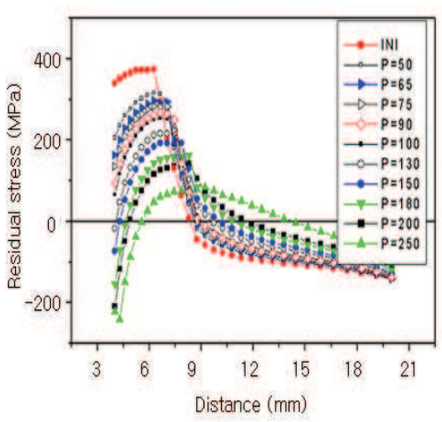

Fig. 6. Residual stress variation by applied loads with stress ratio, R=0

Residual stress relaxation under mechanical loading was studied by the finite element analysis. Mechanical loads were applied to the finite element model shown in figure 1. The plate has initial residual stresses from the welding and hole drilling. Figure 6 shows the residual stress relaxation under a series of loads. The loads increase to the maximum value from zero and decrease linearly to zero.

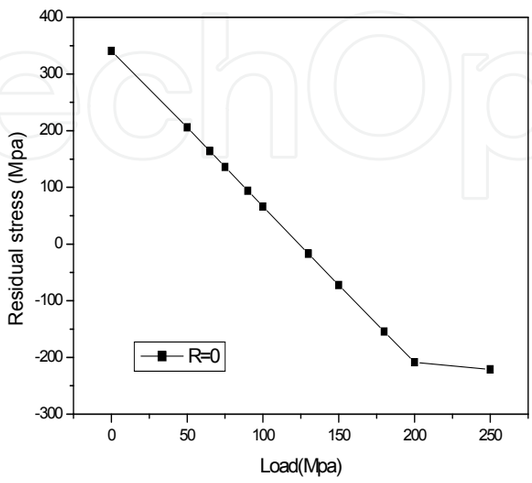

Fig. 7. Variation of residual stress, σ_{yy} at the hole edge by the applied loads

Figure 7 shows the variation of residual stress σ_{yy} at the hole edge (x=4). The residual stress decreases linearly until the applied load increases to 200 MPa. But when the applied load is 250 MPa, the magnitude of the residual stress relaxation is similar to that in case of 200 MPa. When the applied load is 250 MPa, the residual stress after unloading exceeds the compressive yield stress. Figure 8 shows this process. To quantify the effect of the applied loads on the residual stress relaxation, the normalized residual stresses after unloading are represented as a function of the normalized applied loads as shown in figure 9. The relation is expressed as:

$$\sigma_{\mathrm{res}} / \sigma_{\mathrm{res\_ini}} = \mathrm{a}(\sigma_{\mathrm{res\_ini}} + \sigma_{\mathrm{app}}) / \sigma_{\mathrm{y}} + \mathrm{b} \tag{1}$$

where σ_{res} : residual stress after unloading; σ_{res_ini} : initial residual stress; σ_{app} : applied load; σ_{y} : initial yield stress; a, b: constants. a=-0.87 and b=1.88 are obtained. It is found that for the material considered in this study, the welding residual stress, σ_{yy} decreases to zero when $(\sigma_{\mathrm{res\_ini}} + \sigma_{\mathrm{app}}) / \sigma_{\mathrm{y}}$ =2.3.

To examine the behavior of residual stress relaxation in case that fully reversal loads (Load ratio, R=-1) are applied, a tension-compression load of 200 MPa is applied to the same welded specimen used above. In figure 10, the simulation results are shown and compared with the results in case of R=0. The relaxation of the residual stress, σ_{yy} at the hole edge is negligible.

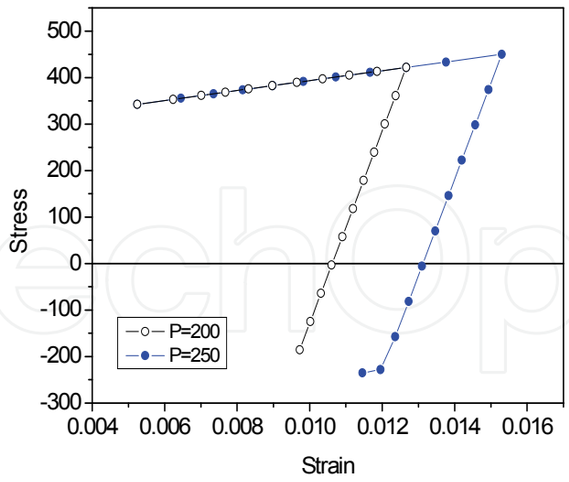

Fig. 8. Finite element analysis of the process of residual stress relaxation

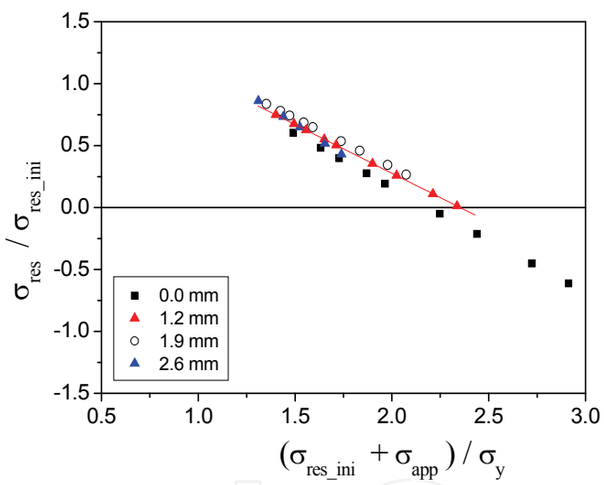

Fig. 9. Normalized residual stresses vs. applied loads. Distance is from the hole edge

From the hole edge to 3mm, the residual stress relaxation occurs. The stress-strain history is shown in figure 11 when the applied load is 200 MPa. Figure 12 shows the simulation results of residual stress relaxation under various applied loads. The residual stress at the hole edge decreases to a certain value and then increases as the applied loads increase. Figure 13 compares the simulation results when R=0 and -1.

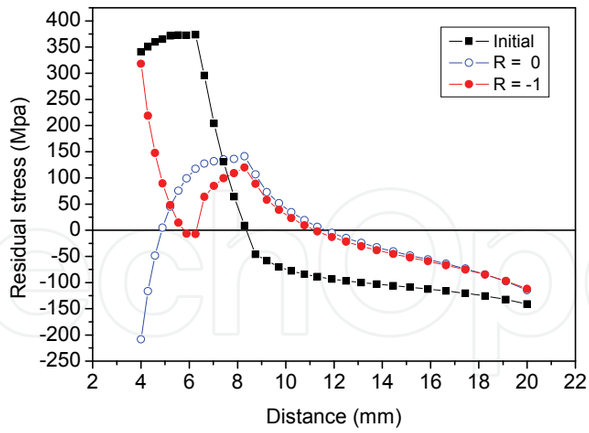

Fig. 10. Effect of stress ratio on the residual stress relaxation. Distance is from the hole center.

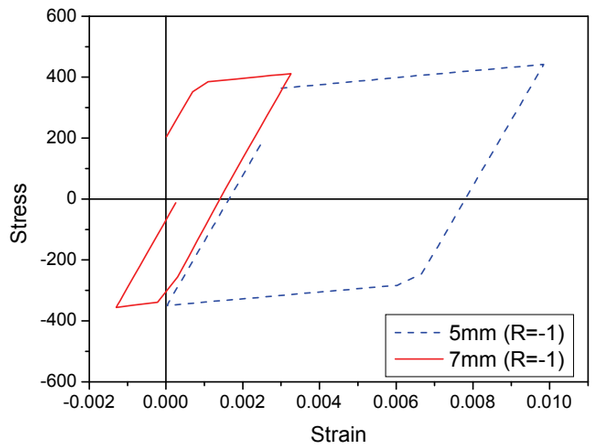

Fig. 11. History of $\sigma - \varepsilon$ under R=-1. Distance is from the hole center.

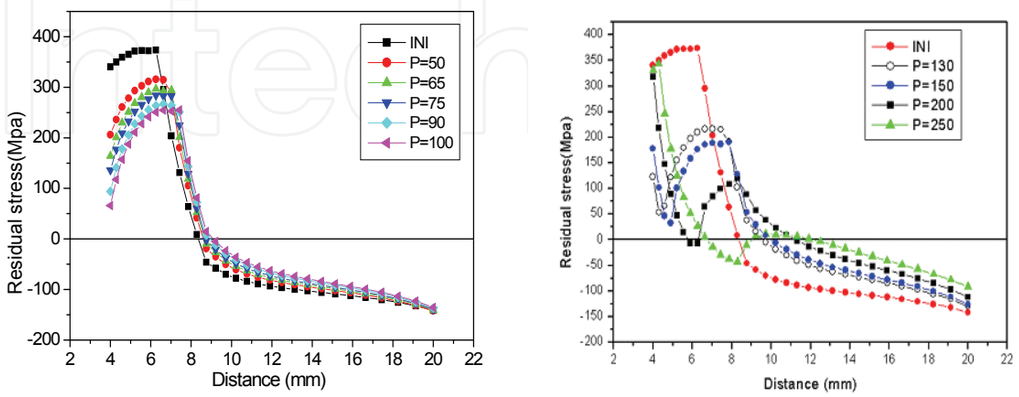

(a) (b)

Fig. 12. Residual stress relaxation in case of R= -1

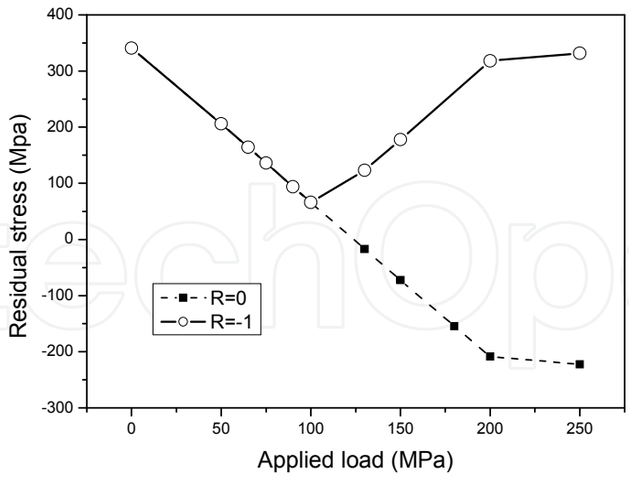

Fig. 13. Residual stress relaxation at the hole edge when R=0 and -1

3. Fatigue crack propagation under residual stresses

In general, cyclic loading is applied to mechanical structures such as rolling stock during the service time, and the structures reach to the final failure due to accumulated fatigue damage. To extend the lifetime of metallic structures under fatigue loading, several methods have been tried, for example extending the time period of crack nucleation or repairing whole section with cracks fully penetrating through the thickness of the section, etc. Song (Song, 2001) has proposed to generate compressive residual stress around the crack tip by heating to retard or stop the fatigue crack growth.

In this chapter, we study the effect of welding residual stresses on fatigue behavior by finite element method. The compact tension specimen is chosen as the analysis object, and the welding line is perpendicular to the direction of the crack propagation. Temperature, residual stress distributions and residual stress redistribution with fatigue crack growth were calculated on the commercial package ABAQUS. There are several procedures for crack growth, for example element extinction, node release and interface-cohesive element, etc. In this paper, to simulate the fatigue crack growth, a cohesive zone model was used along the symmetric line in the crack direction. To account for the damage accumulation due to fatigue, a law of damage evolution was included in the constitutive equation of the cohesive zone model. The analysis was also applied to the specimen not welded. Comparing results obtained from the welded and not-welded specimens, how the residual stresses exert influence on the fatigue behavior was examined.

3.1 Analysis of welding residual stress

To obtain residual stress distribution by welding, it is necessary first to conduct analysis for transient heat transfer, and then obtain mechanical stress distribution from the temperature distribution in the structure. A compact tension (CT) specimen is chosen as the analysis object. Figure 14 shows the two-dimensional finite element modeling of the CT specimen. Only the top half of the full specimen is analyzed by using the symmetry condition to the

center line. The height of the model is 75 mm and the distance between the notch and the right hand side of the specimen (i.e., length of the center line) is 100 mm. Heat input of $3.68\times10^{8} J/m^{2}s$ is applied on the surface of the element along the C-D line from top to bottom with speed of 2.42 mm/s. The distance between the welding line C-D and the notch is 60 mm. Convective boundary condition with ambient temperature ($20^{o}C$) is applied to the boundary lines of the specimen, and heat transfer does not take place across the symmetry line. The material parameters including the latent heat of melting, density variation with temperature, etc. are illustrated in Figure 15. Temperature distribution captured at a time during the welding procedure is illustrated in Figure 16. The maximum temperature is about $1500^{o}C$.

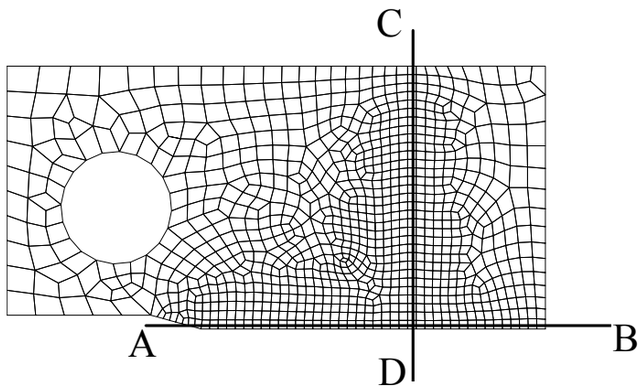

Fig. 14. Finite element mesh for CT specimen. Height of the model is 75mm, and the distance between the notch and the right hand side boundary is 100mm. Along the A-B line, the interface-cohesive elements will be located in the fatigue analyses.

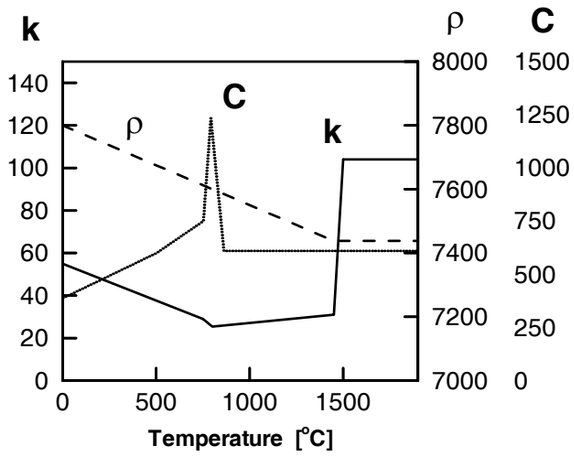

Fig. 15. Variation of conductivity k, density ρ and specific heat C with temperature.

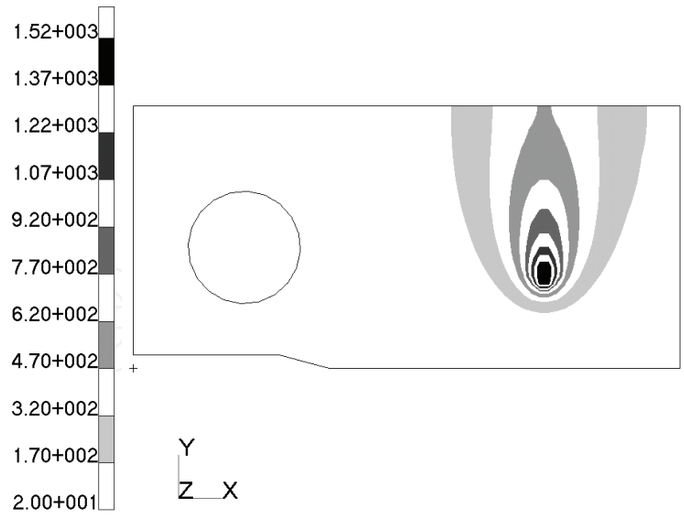

Fig. 16. Temperature distribution at a time during the welding procedure.

The stress distribution induced by the welding was calculated assuming temperature dependent elastic-plastic constitutive behavior for the specimen. The temperature-dependent variation of Young's modulus, Poisson's ratio and approximate strain-hardening behavior of mild steel are given in Figure 17. The resultant residual stress distribution in the CT specimen is shown in Figure 18. It is observed that compressive vertical residual stress, σ_{22}, is generated near the notch by welding. The profiles of the vertical and horizontal residual stresses along the A-B line are drawn in Figure 18 (b). The magnitude of the horizontal residual stress turns out to be small compared to that of the vertical residual stress.

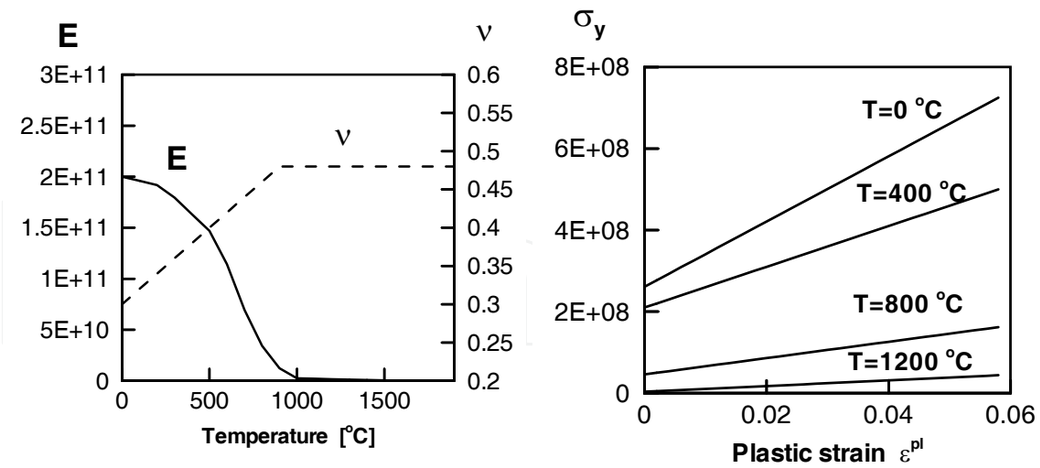

(a) (b)

Fig. 17. (a) Variation of Young's modulus and Poisson's ratio with temperature. (b) Yield strength and plastic strain curves at several temperatures.

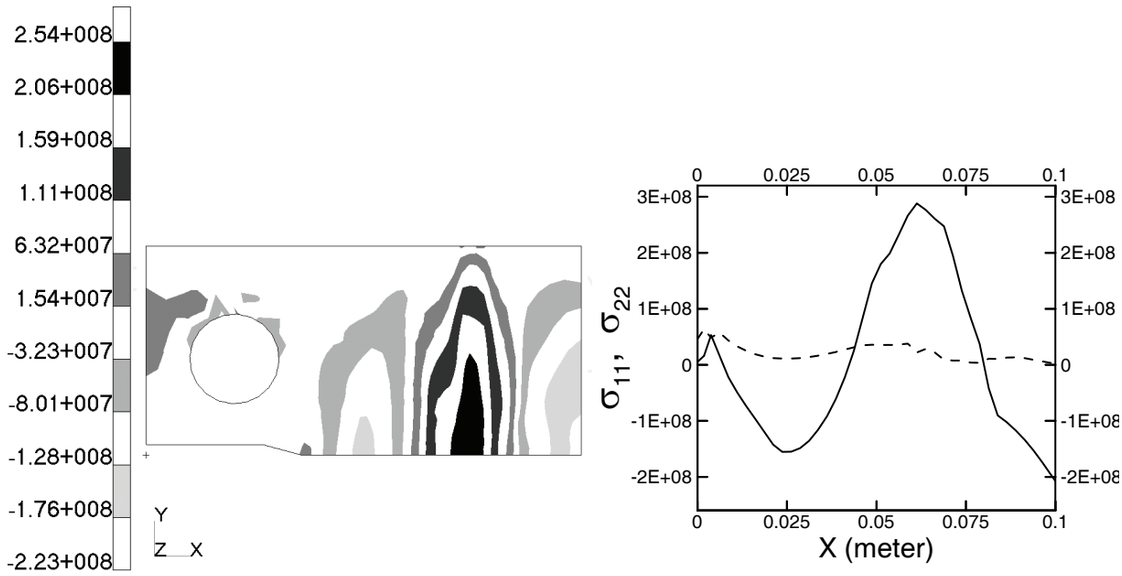

Fig. 18. (a) Vertical residual stress σ_{22} distribution by welding along the C-D line. (b) Welding residual stress σ_{11} and σ_{22} distributions along the A-B line in Figure1; dashed line is σ_{11} and solid line is σ_{22} .

3.2 Cohesive zone model for fatigue crack growth

Cohesive zone models have been developed by many researchers (Needleman, 1987; Rose, Ferrante and Smith, 1981; de-Andres, Perez and Ortiz, 1999). In the viewpoint of cohesive zone model, fracture is regarded as a gradual phenomenon in which separation takes place across an extended crack tip, or cohesive zone, and is resisted by cohesive forces. De-Andres et al. (de-Andres, Perez and Ortiz, 1999) used three-dimensional irreversible cohesive zone model to account for the accumulation of fatigue damage by allowing unloading irreversibility. Roe and Siegmund (2003) developed a constitutive law for the cohesive zone model for fatigue crack growth simulation. In their model, the cohesive forces were reduced by the accumulation of fatigue damage, and a time evolution equation for a damage parameter was used to calculate the current state of damage. Here, we used their time evolution equation of damage to study the fatigue crack growth behavior.

To describe the cohesive laws used in this chapter, we confine our interest in two-dimensional case. An effective traction t is given for a given effective displacement, δ , as follows (de-Andres, Perez and Ortiz, 1999).

$$t = \begin{cases} \lambda\sigma_c \dfrac{\delta}{\delta_c} e^{-\frac{\delta}{\delta_c}} & \text{if } \delta = \delta_{\max} \text{ and } \dot{\delta} \geq 0 \\ \dfrac{t_{\max}}{\delta_{\max}}\delta & \text{if } \delta < \delta_{\max} \text{ or } \dot{\delta} < 0 \end{cases}$$

where $\lambda = \exp(1)$ and σ_c is the cohesive strength of material and δ_c is a characteristic opening displacement. The first equation is for the loading case, and the second one is for unloading case. $\delta_{\max}$ is the maximum attained displacement by loading, and $t_{\max} = t(\delta_{\max})$ in the first equation. In this model, the $t-\delta$ response follows different path for unloading, and the path with unloading is always directed to the origin. For the material separation vector $\boldsymbol{\delta} = \delta_s \mathbf{e}_s + \delta_n \mathbf{e}_n$ where δ_s and δ_n are the sliding and normal opening displacements at the cohesive interfaces, respectively, the effective displacement δ is defined in different ways for normal opening and compression. That is, for normal opening ($\delta_n \geq 0$), the effective displacement and the traction vector are given by

$$\delta = \sqrt{\beta^2 \delta_s^2 + \delta_n^2}$$

$$\boldsymbol{t} = \frac{t}{\delta}\left(\beta^2 \delta_s \mathbf{e}_s + \delta_n \mathbf{e}_n\right)$$

where β is a weighting factor. Meanwhile, for normal compression ($\delta_n < 0$),

$$\delta = \sqrt{\beta^2 \delta_s^2}$$

$$\boldsymbol{t} = \frac{t}{\delta}\beta^2 \delta_s \mathbf{e}_s + t_n \mathbf{e}_n$$

$$t_n = k_s \left.\frac{\partial t}{\partial \delta}\right|_{\delta=0} \delta_n = k_s \lambda \sigma_{c0} \frac{\delta_n}{\delta_c}$$

The last expression means that the cohesive material behaves as a linear spring for normal compression. The stiffness of the compressive spring is taken as a factor k_s times the slope of the effective traction-separation curve at the origin. σ_{c0} is used instead of σ_c to emphasize that the slope is fixed as a constant by the initial value of the cohesive strength. Refer to later sections to see the meaning of varying cohesive strength. The cohesive constitutive equations were implemented using the user interface UEL of ABAQUS.

Figure 19 illustrates loading responses predicted for pure normal displacement and pure sliding by the cohesive traction-separation laws. We can observe that the traction force varies linearly to the displacement in the case of normal compression. The shear traction is symmetric to the origin with the sliding displacement. Meanwhile, if the normal opening and sliding displacements are applied simultaneously, the maximum tensile normal traction resisted by the material will be smaller than the cohesive strength of material, σ_c.

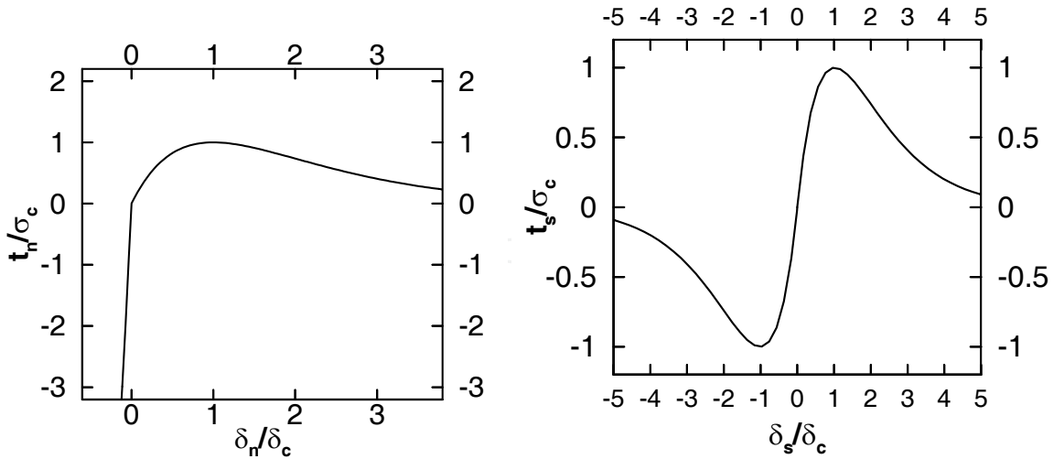

(a) (b)

Fig. 19. (a) Normal traction vs. normal displacement relation with $\delta_s = 0$. (b) Shear traction vs. shear displacement relation with $\delta_n = 0$.

With the cohesive constitutive equations described above, cyclic loading with the maximum traction below the cohesive strength will result in infinite life. To establish a cohesive zone model that can capture finite life effects, the cohesive zone constitutive equations should include evolving cohesive properties with time. Roe and Siegmund (Roe and Siegmund, 2003) applied damage mechanics to the development of an evolution equation for a damage parameter. The damage parameter was incorporated into the traction-separation law via the cohesive traction. That is, the cohesive constitutive equation for damage accumulation under cyclic loading is given by using the current cohesive strength defined by

$$\sigma_c = (1 - D)\sigma_{c0}, \qquad 0 \le D \le 1$$

where D is the damage parameter, and σ_{c0} is the initial cohesive strength. To compute the current state of damage, a damage evolution equation was proposed as follows.

$$\dot{D} = \frac{|\dot{\delta}|}{\delta_D}\left(\frac{t}{\sigma_c} - \frac{\sigma_f}{\sigma_{c0}}\right) H\left(\bar{\delta} - \delta_f\right), \qquad \dot{D} \ge 0$$

where H denotes the Heavyside function, $\bar{\delta} = \int |\dot{\delta}| dt$, σ_f is an endurance limit below which cyclic loading can proceed infinitely without failure, and δ_D, δ_f are positive material constants. $|\dot{\delta}|$ is defined by

$$\left|\dot{\delta}\right| = \begin{cases} \sqrt{\beta^2 \dot{\delta}_s^2 + \dot{\delta}_n^2} & \text{for } \delta_n \geq 0 \\ \sqrt{\beta^2 \dot{\delta}_s^2} & \text{for } \delta_n < 0 \end{cases}.$$

3.3 Results of fatigue crack growth simulation

To investigate the effect of welding residual stress on fatigue behavior, compact tension (CT) specimens with and without residual stresses are analyzed by two-dimensional plane strain finite elements with thickness 1m. By symmetry of the problem only top half of the specimen is analyzed, and the cohesive interface elements are located along the symmetry line in the crack propagation direction. The material data used for the cohesive laws in this investigation are listed in Table 1. The values are presumed approximately, and they need to be calibrated by comparing with experimental works in the future. The surrounding matrix is modeled by elastic-plastic solid. The material properties of welded specimen can be different from toes of not-welded specimen because the microstructures are changed by welding. But, in this computational work, the same material properties are assumed before and after welding.

First, Figure 20 and Figure8 illustrate results of fatigue crack growth simulation of the specimen without welding residual stress. Repeated triangle type displacement loading oscillating between 0 and the maximum amplitude of 0.1 mm with period of 2 seconds was applied vertically at the top point of the hole in the CT specimen. The crack extension with respect to time is shown in Figure7. In this case, the level of the applied traction to the cohesive zone is less than the cohesive strength of the material, but as the cyclic loading proceeds fatigue crack propagates. The slope of the crack extension-time curves were determined for a series of the stress intensity ranges $\frac{da}{dN} = C\Delta K^n$ at a point (15 mm away from the notch along the A-B line) and plotted in a log-log scale. Circles in Figure 21 summarize these data. To obtain the value of the stress intensity factor, the mathematical formula (Anderson, 1995) or finite element analysis can be used. In this work, ABAQUS option **contour integral* was used to compute the stress intensity factor, and the result was almost the same as that by the formula. The numerically predicted data could be fitted to a Paris type power law $da/dN = C\Delta K^n$ with $n \approx 3.32$. Figure 22 illustrates the vertical stress σ_{22} distribution generated during the fatigue crack growth in load control simulation in which maximum point force of 5 MN is applied periodically at the top point of the hole. Small amount of compressive residual stress is induced behind the crack tip which causes closure of crack surfaces.

Next, to investigate fatigue behavior under the welding residual stress, specimen with the welding residual stress distribution obtained in the previous section was tested for cyclic point force loading with amplitude 5 MN. Figure 23 shows redistributions of welding residual stress with the fatigue crack propagation. Compressive vertical stress σ_{22} is redistributed as the fatigue crack grows into the CT specimen. To satisfy the equilibrium condition the tensile residual stress is also relaxed by little amount. In the figure, the position of crack tip corresponds to the location where $D = 0.5$. Triangles in Figure8 plot

the crack growth rate-$\frac{da}{dN} = C\Delta K^n$ behavior on a log-log scale for the case with welding residual stress. ($\frac{da}{dN} = C\Delta K^n$ is the values calculated for the specimen without welding residual stress.) As seen in the plot, the computation predicts reduction of the crack growth rate for the case with welding residual stress. One can expect that crack closure takes place by the compressive vertical welding residual stress, and the effective traction in the cohesive zone should be reduced. In this case, the effective stress intensity factor ΔK_{eff}, which is defined by the difference between ΔK and the stress intensity at which the crack opens, is less than ΔK, and the crack growth rate is expected to decrease.

σ_{c0}	1000 [M Pa]	δ_D	0.5 [mm]
δ_c	0.05 [mm]	σ_f	150 [M Pa]
δ_f	0.25 [mm]	k_s	2

Table 1. Numerical parameters for the cohesive zone model.

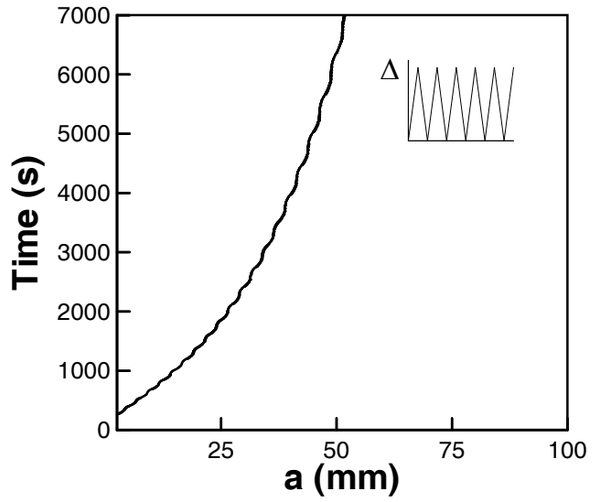

Fig. 20. Numerical fatigue crack growth result for constant amplitude fatigue without residual stress. Amplitude of the cyclic displacement loading was 0.1 mm. 7000 seconds corresponds to 3500 cycles.

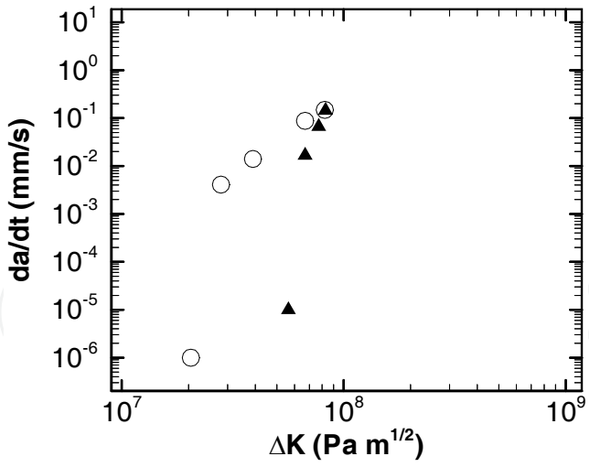

Fig. 21. Numerical fatigue crack growth rates with and without welding residual stress. Circles are results without welding residual stress, and triangles are results with welding residual stress

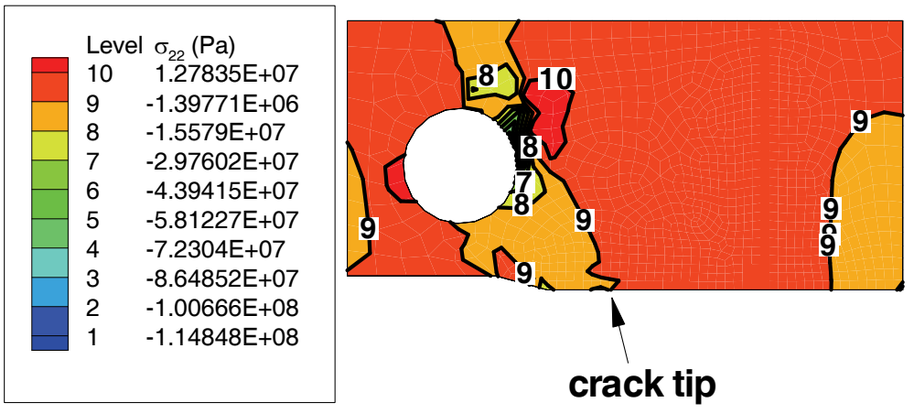

Fig. 22. Vertical residual stress σ_{22} distribution after 125 cycles. Vertical point force is applied periodically at the top of the hole. This analysis is for the case without welding residual stress. Behind the crack tip, small amount of compressive residual stress is generated.

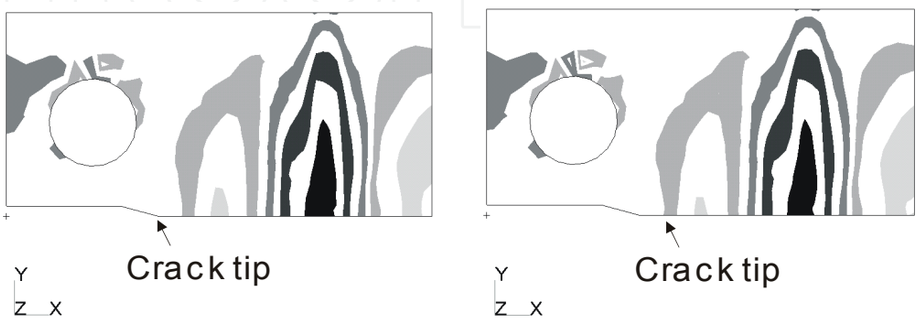

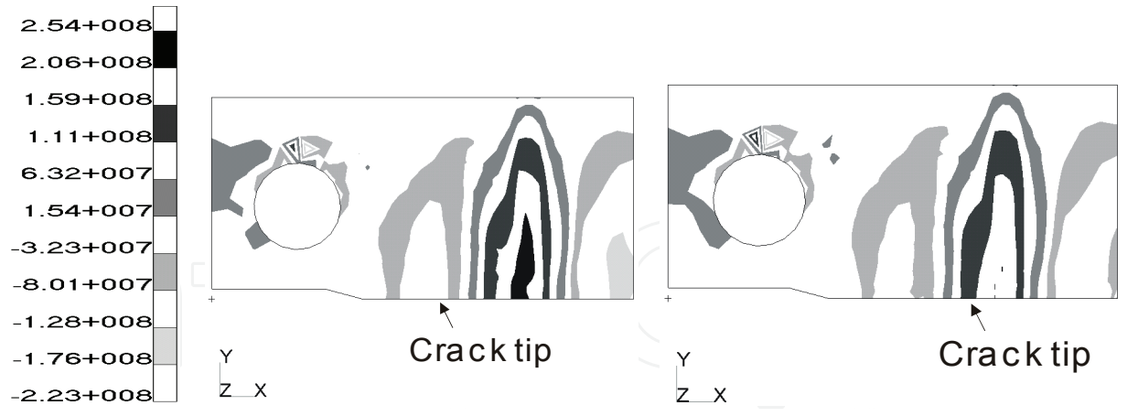

(c) (d)

Fig. 23. Redistributions of welding residual stress σ_{22} with the crack growth. The contour plots are drawn at external-loading-free-states. Location of the crack tip is marked at each case. (a) After 50 cycles. (b) After 100 cycles. (c) After 200 cycles. (d) After 250 cycles.

4. Fatigue life estimation considering residual stresses

Residual stresses play a significant role in structural behavior of welded joints. According to our tensile fatigue tests at 20 Hz, R=0.1 on butt-welded joints, fatigue strength of as-welded specimens, that is, specimens having residual stress is higher than that of annealed specimens in the short life, but vice verse in the long life (Figures 24, 25).

To simulate this behavior, taking into account the residual stress relaxation and notch effect, we developed a model to evaluate fatigue lives of welded joints with residual stresses. To evaluate the fatigue lives of welded structures by a strain-life approach, it is necessary to identify the value of parameters through tests or literature. But it is difficult for field engineers to get the necessary data through tests from the viewpoint of time and cost. Therefore, some researchers (Lida, 2001; Reemsnyder, 1981; Lawrence, Burk and Yung, 1982) have been studying to obtain fatigue properties from simple tensile tests and hardness measurement. We surveyed literature and quoted a procedure to identify the fatigue parameters for fatigue life evaluation based on a local strain approach.

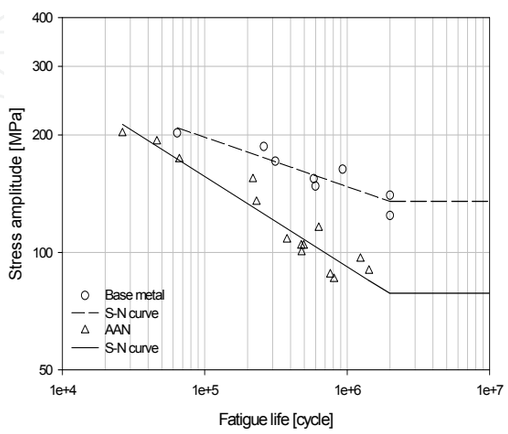

Fig. 24. S-N curves for base material and as-welded (AAN) specimens

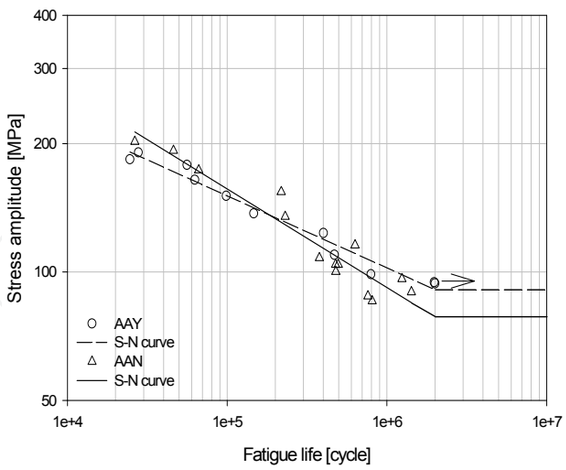

Fig. 25. S-N curves for annealed (AAY) and not annealed (AAN)

4.1 Relations between mechanical and fatigue properties

When mean stress effect is neglected, one of the equations frequently used for local strain-life approach is Coffin-Manson's (Vormwald and T. Seeger, 1987; Stephens, Fatemi, Stephens and Fuchs, 2001)

$$\frac{\Delta\varepsilon}{2} = \frac{\Delta\varepsilon_e}{2} + \frac{\Delta\varepsilon_p}{2} = \frac{\sigma'_f}{E}(2N_f)^b + \varepsilon'_f(2N_f)^c \tag{1}$$

Where $\Delta\varepsilon/2$, $\Delta\varepsilon_e/2$ and $\Delta\varepsilon_p/2$ are total, elastic and plastic strain amplitude respectively. σ'_f, ε'_f, b and c are constants. N_f is the number of cycles to failure. Roessle and Fatemi (Lawrence, J. D. Burk and J. Y. Yung, 1982) obtained σ'_f and ε'_f as a function of Brinell hardness, HB and/or Young's modulus, E:

$$\sigma'_f = 4.25HB + 225 \text{ (MPa)}; \quad \varepsilon'_f = \frac{0.32(HB)^2 - 487HB + 191000}{E} \tag{2a, b}$$

And using b =-0.09 and c =-0.56, they expressed Eq. (1) with the Brinell hardness and Young's modulus:

$$\frac{\Delta\varepsilon}{2} = \frac{4.25HB + 225}{E}(2N_f)^{-0.09} + \frac{0.32(HB)^2 - 487HB + 191000}{E}(2N_f)^{-0.56} \tag{3}$$

To consider mean stress effect, we express Basquin's equation as a following formula:

$$\sigma_{max} = \Delta\sigma / 2 = \sigma'_f (2N_f)^b \tag{4}$$

where $\sigma_{\max}$ is maximum local stress. Multiplying Eq. (3) by Eq. (4), we obtain a parameter expressed as a function of the Brinell hardness and Young's modulus:

$$\frac{E\sigma_{\max}\Delta\varepsilon}{2} = (4.25HB+225)^2(2N_f)^{-0.18} + (4.25HB+225)[-0.32(HB)^2 - 487HB + 191000](2N_f)^{-0.65} \tag{5}$$

4.2 FE model and fatigue notch factors

We evaluated the fatigue lives of four kinds of specimens with a width of 25 mm (Figure 26) at a stress ratio of $R = 0.1$. The weld bead profiles necessary for modeling were measured on a contour measuring instrument, Mitutoyo CV-3000S4, with a resolution of 0.0002 mm. FE models are shown in Figure 27. A half of the specimen is considered. The obtained stress concentration factors, K_t, by FE analysis and fatigue notch factors, K_f, by Peterson's formula [Stephens, Fatemi, Stephens and Fuchs, 2001) are shown in Table 2.

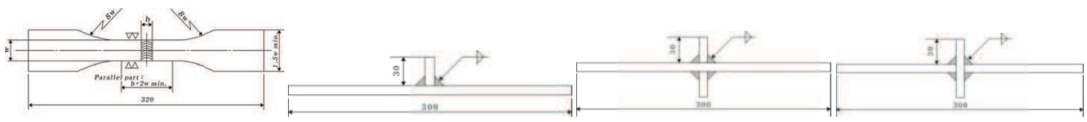

(a) Butt-welded (b) TN (c) NCN (d) CN

Fig. 26. Specimens for fatigue tests and FE analysis

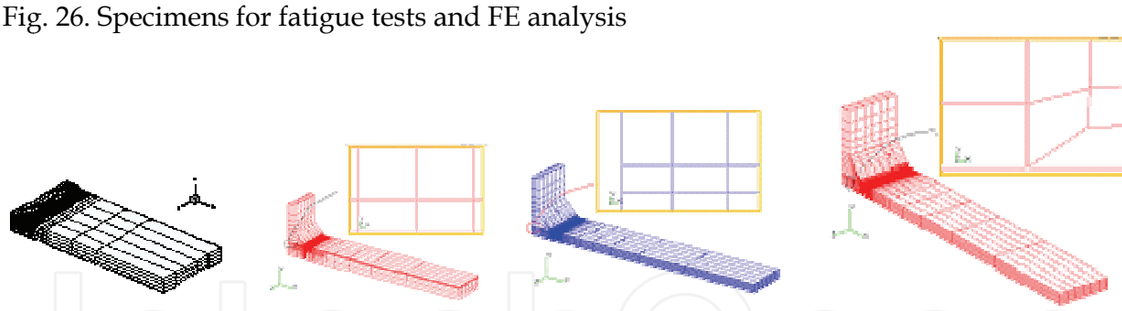

(a) Butt-welded (b) TN (c) NCN (d) CN

Fig. 27. FE analysis models

Specimens	Butt-weld	TN	NCN	CN
K_t / K_f	1.60/1.52	2.71/1.63	3.64/1.93	4.22/2.40

Table 2. Calculated stress concentration factors and fatigue notch factors

4.3 FE analyses of residual stress and residual stress relaxation

The analyses of welding residual stress and residual stress relaxation were carried out on ABAQUS. Weld beads are generated by the element birth technique supplied on ABAQUS. The input data for welding is shown in Table 3 and material constants such as density, ρ,

conductivity, C, specific heat, k, Young's modulus, E, Poisson's ratio, ν (Davis, 1990), plastic strain-yield strength relationship, ε_{pl} - σ_y, used for the FE analyses are shown in Figure 28. They are dependent on temperature.

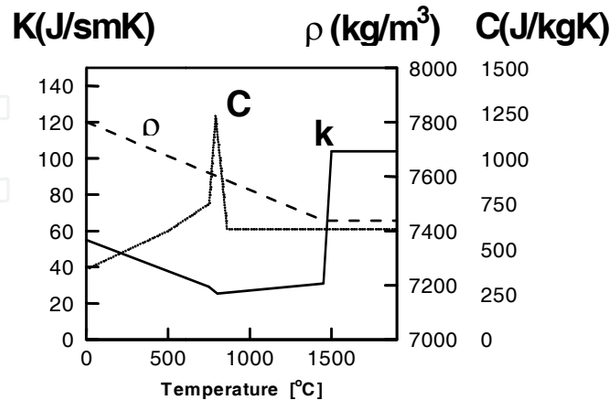

(a) ρ, C, k

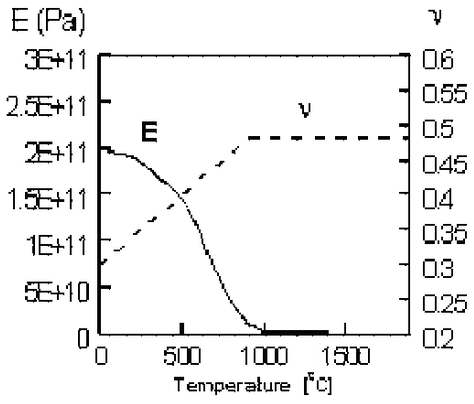

(b) E, ν

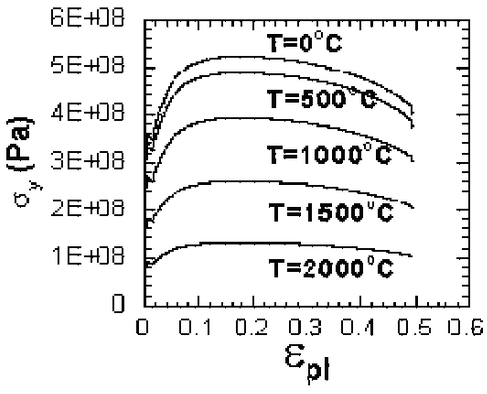

(c) ε_{pl} - σ_y

Fig. 28. Material properties used for FE analysis

Parameters	Filler metal temp. [°C]	Solidus temp. [°C]	Liquidation latent heat [°C]	Arc efficiency	Voltage [V]	Current [A]	Arc beam radius [m]	Heat convection coefficient [J/sm²°C]
Butt-weld	2000	1465	1544	0.4	105	150	0.005	10
TN,NCN,CN	2000	1465	1544	0.4	28	270	0.005	10

Table 3. Parameters for weld analysis

Figure 29 shows the residual stress relaxation by an applied loading at a stress ratio R =0.1. The loading increases linearly to $S_{\max}$ and decreases linearly to $S_{\min}$. The positions A and D are shown in Figure 30.

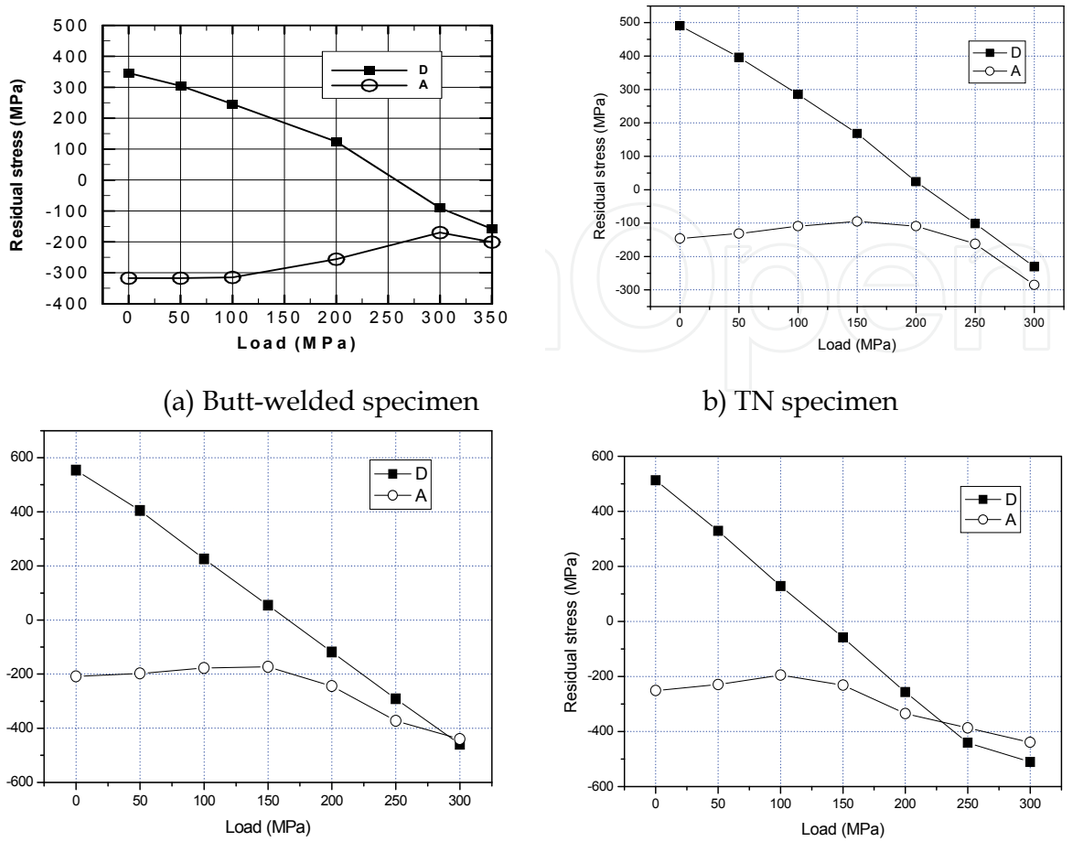

Fig. 29. Residual stress relaxation at A and D by applied loading

Fig. 30. Locations A and D in Figure6 for the residual stress relaxation

The initial residual stress, σ_{11} (σ_{xx}), due to welding is tensile in the middle part of the specimen (near D, F, G), while compressive near the edge (near A, B, C). When the external loading is applied, the residual stresses are redistributed. At point D, the residual stress, σ_{11}, decreases with the applied loading. When the applied load, $S_{\max}$, is greater than a certain value, the residual stress at point D changes to compressive residual stress for all specimens. At point A, the residual stress, σ_{11}, increases to a certain value with the applied loading and then decreases. In case of the CN specimen, the residual stress at point A becomes larger than the residual stress at point D when the applied loading is larger than about 230 MPa. When the applied load is less than 230 MPa, cracks will begin at point D. But the applied load is larger than 230 MPa, cracks will begin at point A. This means the

locations of fatigue crack initiation depend on the magnitude of applied load.

4.4 Fatigue life evaluation of welded joints

We applied Eq. (5) to evaluate the fatigue lives of four kinds of welded joints aforementioned. We measured micro Vickers hardness of the butt-welded specimens with 5kg loading. Figure 31(a) shows the measuring points. Fatigue failure occurs at the notch roots located near the boundary of the weld metal and heat-affected zone. In this area, the Vickers hardness is about 150. The measured Brinell hardness ranged from 147 to 156 HB. For the evaluation of fatigue lives, we used the Brinell hardness 150 HB. Figures 32-35 show the predicted and experimental results. The experimental results were obtained from as-welded specimens. The predicted results with residual stress were obtained by considering the maximum initial residual stress obtained during the welding analysis above-mentioned. In case of the predicted results without residual stress, the initial residual stress was assumed to be zero. In the short life, the effect of residual stress on the fatigue strength is less than that in the long life. This means when the applied load is high, the initial residual stress relaxes much. But when the applied load is low, the mechanical behavior of the notches is elastic. In this case the residual stress plays a role as a mean stress.

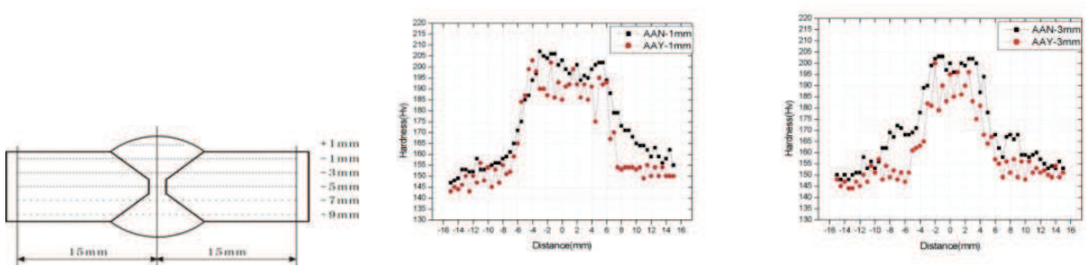

(a) Measured points (b) Hardness at depth –1 m (c) Hardness at depth –3 mm

Fig. 31. Micro Vickers hardness

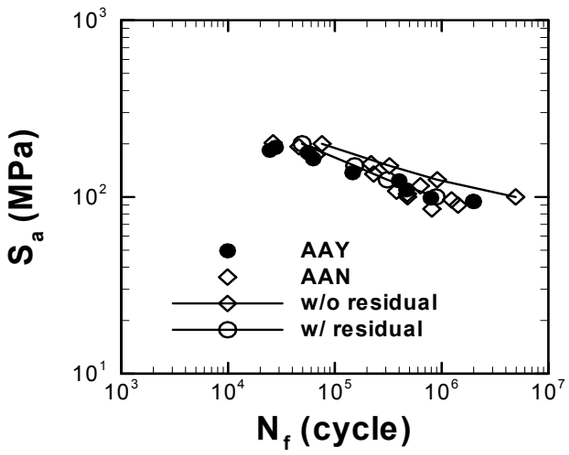

Fig. 32. Butt weld

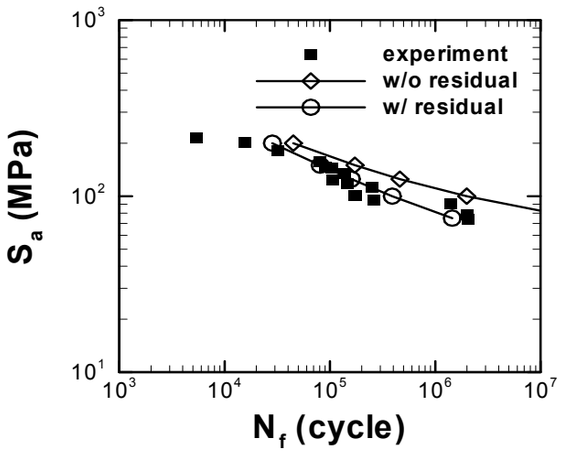

Fig. 33. T-shape fillet weld

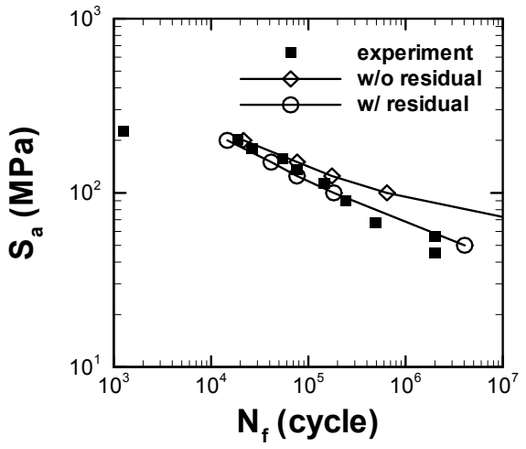

Fig. 34. Non load carrying cruciform

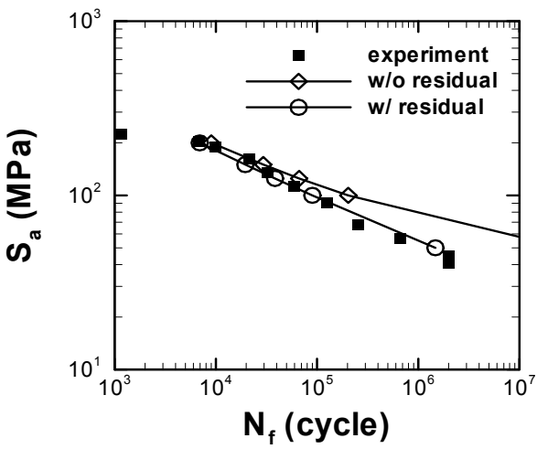

Fig. 35. Load carrying cruciform

5. Conclusions

Residual stresses play an important role in the behavior of welded components and structures. How to deal with them has been one of the challenging problems for engineers and researchers. One of the useful methods to relieve the residual stresses is to apply mechanical loading. When a cyclic zero-maximum mechanical load (R=0) is applied to a specimen with initial tensile residual stresses, the tensile residual stresses are relaxed if the sum of the applied load and initial residual stresses is big enough to produce yielding of the material. The tensile residual stresses may even change to compressive residual stresses. When a fully reversal load (R=-1) is applied to the same specimen, the effect of the residual stress relaxation is not significant. The applied compressive loads produced the tensile residual stresses. The process of residual stress relaxation can be simulated successfully by the finite element method.

The effect of welding residual stresses on fatigue behavior can be simulated too by the finite element method. We modeled the fatigue crack propagation under cyclic loading for two-dimensional compact tension specimens with and without welding residual stress. Initial welding residual stress was generated by conducting transient thermo elastic-plastic finite element analyses. Then a cohesive zone model with evolutionary damage law was applied to predict the fatigue crack growth under the residual stress. When compressive residual stress normal to the crack surface existed around the crack tip, the fatigue crack growth rate was slower. As the fatigue crack propagates, the welding residual stresses are redistributed.

When estimating structural strength or fatigue life, residual stresses should be also considered. We proposed a parameter for fatigue life evaluation considering residual stress. According to the results, the locations of fatigue crack initiation depend on the magnitude of applied load, because residual stresses are redistributed, which change the weakest point under applied loading. The predicted results are in a better agreement with experimental results when we consider the welding residual stresses.

6. References

Iida, K. and Takanashi, M., Welding in the World, **Vol.41**, 314 (1998).
Yang, S. Y. and Goo, B. C. (2005). Key Engineering Materials, Vol. 297~300, p. 710.
Goo, B. C., Yang, S. Y. and Seo, J. W. (2005). Key Engineering Materials, Vol. 297~300, p. 762.
Song, H. C. (2001). Ph.D. thesis, Seoul National University, Korea.
Needleman, A. (1987). J. Appl. Mech. Vol. 54, p. 525.
Rose, J. H., Ferrante, J. and Smith, J. R. (1981). Phy. Rev. Let., Vol. 47, p. 675.
De-Andres, A., Perez, J. L. and Ortiz, M. (1999). Int. J. Sol. Struct., Vol. 36, p. 2231.
Roe, K. L. and Siegmund, T. (2003). Eng. Fract. Mech., Vol. 70, p. 209.
Anderson, T. L. (1995). Fracture Mechanics, CRC Press, U.S.A.
Reemsnyder, H. (1981). Experimentation and Design in Fatigue, pp. 273-295.
Lawrence, F. V., Burk, J. D. and Yung, J. Y. (1982). ASTM STP 776, pp. 33-43.
Vormwald, M. and Seeger, T. (1987). Residual stresses in Science and Technology, pp. 743-750.
Stephens, R. I., Fatemi, A., Stephens, R. R. and Fuchs, H. O. (2001). Metal Fatigue in Engineering, John Wiley & Sons, Inc., pp. 196-205.
Davis, J. R. (1990). Materials Handbook, 10th edition, Vol. 1, American Society for Metals, U.S.A.

IntechOpen

Finite Element Analysis

Edited by David Moratal

ISBN 978-953-307-123-7

Hard cover, 688 pages

Publisher Sciyo

Published online 17, August, 2010

Published in print edition August, 2010

Finite element analysis is an engineering method for the numerical analysis of complex structures. This book provides a bird's eye view on this very broad matter through 27 original and innovative research studies exhibiting various investigation directions. Through its chapters the reader will have access to works related to Biomedical Engineering, Materials Engineering, Process Analysis and Civil Engineering. The text is addressed not only to researchers, but also to professional engineers, engineering lecturers and students seeking to gain a better understanding of where Finite Element Analysis stands today.

InTech Europe

University Campus STeP Ri
Slavka Krautzeka 83/A
51000 Rijeka, Croatia
Phone: +385 (51) 770 447
Fax: +385 (51) 686 166
www.intechopen.com

InTech China

Unit 405, Office Block, Hotel Equatorial Shanghai
No.65, Yan An Road (West), Shanghai, 200040, China
中国上海市延安西路65号上海国际贵都大饭店办公楼405单元
Phone: +86-21-62489820
Fax: +86-21-62489821

IntechOpen